




Cite this: *RSC Adv.*, 2017, 7, 44884

# Unexpected stable stoichiometries and superconductivity of potassium-rich sulfides†‡

Ying Li,  Xilian Jin, \* Tian Cui, \* Quan Zhuang, Die Zhang, Xing Meng, Kuo Bao, Bingbing Liu  and Qiang Zhou

Alkali metal compounds exhibit novel characteristics under pressure, such as antimetallization in  $\text{CLi}_4$ , high superconductivity at 80 K in highly compressed  $\text{Li}_3\text{S}$ , and the existence of unexpected stable stoichiometries of sodium chlorides, etc., which have greatly prompted us to explore  $\text{K}_x\text{S}$  compounds at pressure. We found several stable structures with a variety of stoichiometries and proposed a phase diagram on the K-rich side first. Chemical rules established at ambient pressure are frequently violated when high pressure is applied,  $\text{Na}_3\text{Cl}$  and  $\text{NaCl}_3$  as unusual stoichiometries of sodium chloride have been reported in high-pressure conditions. However,  $\text{KS}$ , with its counterintuitive chemical formula, has been discovered theoretically even at ambient pressure, and possesses the same stability as  $\text{K}_2\text{S}$ . The mechanism of superconductivity in  $Pm\bar{3}m$   $\text{K}_3\text{S}$  is deeply investigated, comparing with the reported  $Pm\bar{3}m$   $\text{Li}_3\text{S}$ . The weak electron–phonon coupling mainly contributes to the weak superconductivity in  $\text{K}_3\text{S}$ , which is fully in contrast to the mechanism of interstitial charge localization which dominates the low  $T_c$  in the reported  $\text{Li}_3\text{S}$ .

Received 6th July 2017  
Accepted 22nd August 2017

DOI: 10.1039/c7ra07455g

rsc.li/rsc-advances

## Introduction

Recently, alkali metal compounds have revived the interest of the scientific community to explore their novel structures and characteristics upon compression. Different Na–Cl compounds such as  $\text{Na}_3\text{Cl}$ ,  $\text{Na}_2\text{Cl}$ ,  $\text{Na}_3\text{Cl}_2$ ,  $\text{NaCl}_3$ , and  $\text{NaCl}_7$  are thermodynamically stable at nonambient pressure conditions which contrasts the familiar rules of chemistry.<sup>1,2</sup> The compound of helium and sodium,  $\text{Na}_2\text{He}$ , reported recently has changed the hitherto bare field of helium chemistry, providing new twists to the chemistry of noble gases.<sup>3</sup> Antimetallization is predicted in the dense lithium-rich compound  $\text{CLi}_4$  (ref. 4) which means that this phenomenon is expected in not only alkali metals  $\text{Li}^{3-7}$  and  $\text{Na}^8$  but also multiple compounds. Interestingly, superconductivity is predicted in alkali metal compounds such as a Li–S system, and  $T_c$  has risen to 80 K in highly compressed  $\text{Li}_3\text{S}$ .<sup>9</sup>

Alkali metal sulfides are characterized by their high ionic conductivity and large band gap. They appear to be promising candidates for technological applications in solid state batteries, fuel cells and solid state gas-detectors.<sup>10,11</sup> The properties of alkali metal sulfides of  $\text{X}_2\text{S}$  ( $\text{X} = \text{Li}, \text{Na}, \text{K}, \text{or Rb}$ ) have been explored thoroughly, including phase sequence, elastic properties, electronic structure, optical properties, etc.<sup>12–20</sup> The

conventional superconductivity in the phase diagram of the Li–S system has been explored by *ab initio* methods for crystal structure prediction and linear response calculations for electron–phonon coupling.<sup>9</sup> Most of these phases are metallic, but they exhibit no or low- $T_c$  superconductivity, except for the  $Fm\bar{3}m$  space group of  $\text{Li}_3\text{S}$  with a  $T_c$  of 80 K at 500 GPa. In contrast to the low- $T_c$  of  $Pm\bar{3}m$   $\text{Li}_3\text{S}$ , it is concluded that interstitial charge localization due to avoiding core overlap can be a fundamental limiting factor for conventional superconductivity.

In this work, various stoichiometric structures of  $\text{K}_x\text{S}$  ( $x = 1-4$ ) systems are widely investigated up to 100 GPa. We found six thermodynamically stable structures with the stoichiometries of  $\text{KS}$ ,  $\text{K}_3\text{S}$  and  $\text{K}_4\text{S}$  under these conditions and proposed a phase diagram on the K-rich side first.  $\text{KS}$ , the totally counterintuitive chemical formula with extraordinary bonding and electronic properties, is predicted to be stable at atmospheric pressure in  $\text{K}_x\text{S}$  compounds. The mechanism of superconductivity in  $Pm\bar{3}m$   $\text{K}_3\text{S}$  is deeply investigated and compared with the reported  $Pm\bar{3}m$   $\text{Li}_3\text{S}$ . The low  $T_c$  is attributed to a weak interaction of electron–phonon coupling in the  $\text{K}_3\text{S}$  compound instead of interstitial charge localization like in the reported  $\text{Li}_3\text{S}$  compound.<sup>9</sup>

## Computational methods

The structural prediction for the  $\text{K}_x\text{S}$  compounds at different pressures was performed by the ELocR code.<sup>21</sup> The high accuracy structural relaxations and electronic localization functions (ELF) were performed using density functional theory with the

College of Physics, State Key Laboratory of Superhard Materials, Jilin University, Changchun, 130012, People's Republic of China. E-mail: jinxilian@jlu.edu.cn; cuiitian@jlu.edu.cn

† Dedicated to Prof. Guangtian Zou on the occasion of his 80<sup>th</sup> birthday.

‡ Electronic supplementary information (ESI) available. See DOI: 10.1039/c7ra07455g



Vienna ab initio simulation package (VASP).<sup>22</sup> The Perdew–Burke–Ernzerhof (PBE) generalized gradient approximation (GGA)<sup>23</sup> was selected for the exchange–correlation function. The partial augmented wave (PAW)<sup>24</sup> method was adopted with the PAW potentials where  $s^2p^4$  and  $3s^3p^4s$  are treated as valence electrons. Brillouin zone sampling used a grid spacing of  $2\pi \times 0.03 \text{ \AA}^{-1}$  and the plane-wave cutoff energy was 600 eV.

The electronic projected density of states and the electronic band structure were calculated by the CASTEP<sup>25</sup> code with a cutoff energy of 720 eV, norm-conserving pseudopotentials, GGA-PBE exchange–correlation functional, and Brillouin zone sampling grid with a spacing of  $2\pi \times 0.04 \text{ \AA}^{-1}$ . The dynamic properties, three-dimensional Fermi surfaces and electron–phonon coupling calculations were studied in the QUANTUM-ESPRESSO package.<sup>26</sup> The Troullier–Martins-type norm-conserving pseudopotentials were used, and convergence tests provided a suitable value of 60 Ry for the kinetic energy cutoff. The q-point meshes in the first Brillouin zone of  $8 \times 8 \times 8$  for  $Pm\bar{3}m$  ( $\text{Li}_3\text{S}$ ) and  $4 \times 4 \times 4$  for  $Pm\bar{3}m$  ( $\text{K}_3\text{S}$ ) were used for phonon and electron–phonon calculations.

## Results and discussion

We have systematically studied the chemical stabilities of various  $\text{K}_x\text{S}$  ( $x = 1\text{--}4$ ) compounds by calculating the enthalpies of formation up to 100 GPa. The thermodynamical stability of different compounds with respect to elemental K and S solids at each pressure is calculated using the equation below:

$$\Delta H(\text{K}_x\text{S}) = [H(\text{K}_x\text{S}) - xH(\text{K}) - H(\text{S})]/(x + 1)$$

where  $\Delta H$  is the enthalpy of formation per atom and  $H$  is the calculated enthalpy per chemical unit for each compound. All possible structures with lower enthalpies are provided in the convex hull, as shown in Fig. 1 and S1.†

According to the hull data, a compound lying on the convex hull is thermodynamically stable with respect to decomposition

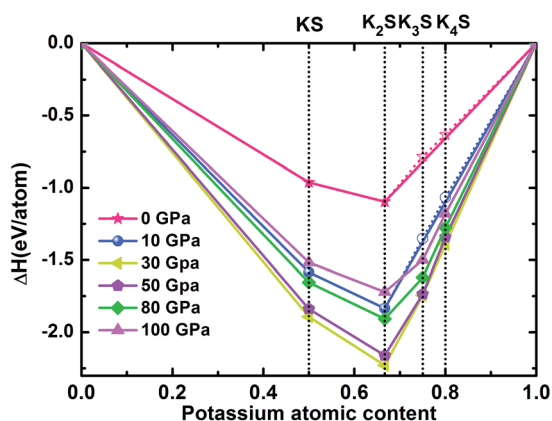


Fig. 1 Enthalpy difference curves of  $\text{K}_x\text{S}$  with respect to K and S at selected pressures. The  $\text{K}_x\text{S}$  structures on the convex hull (solid lines) are thermodynamically stable relative to decomposition into other  $\text{K}_x\text{S}$  compounds and elements, whereas those located above the convex hull (dashed lines) are unstable or metastable.

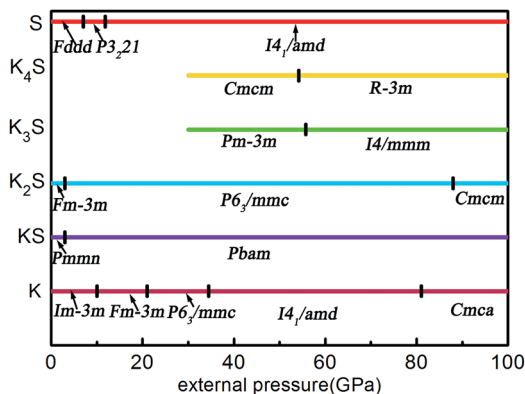


Fig. 2 The phase diagram of the  $\text{K}_x\text{S}$  system in the stable pressure range.

into other K–S compounds or elemental K and S solids, and thus it is experimentally synthesizable. However, those located above the convex hull indicated by dashed lines are either unstable or metastable. In order to obtain clear information for the structures at ambient conditions and 10 GPa, the independent convex hull is shown in Fig. S1.† Moreover, the phase diagram for the  $\text{K}_x\text{S}$  crystals is presented in Fig. 2.

Under ambient conditions, the stable phase of KS crystallizes in the orthorhombic structure of  $Pm\bar{m}n$  and remains stable until 3 GPa as shown in Fig. 3(a). There are three nonequivalent atoms, and the nearest distance between K and S is 3.16 Å. K atoms occupy the crystallographic 2b position with  $mm2$  symmetry on the top and bottom sides, and the other nonequivalent K atoms occupy the crystallographic 2a position with  $mm2$  symmetry in the middle of the crystal. S atoms occupy the crystallographic 4f position with  $.m$  symmetry. Elevating the pressure above 3 GPa, another orthorhombic phase with  $Pbam$  symmetry emerges which is stable until 100 GPa, as depicted in Fig. 3(b). There are two nonequivalent atoms in the crystal lattice, and they consist of one KS unit. K atoms occupy the crystallographic 4h position with  $.m$  symmetry, and S atoms occupy the crystallographic 4g position with  $.m$  symmetry. The nearest distance between K and S is 2.558 Å. As for  $\text{K}_3\text{S}$  and  $\text{K}_4\text{S}$ , they are thermodynamically metastable under normal conditions until 30 GPa. With increasing pressure,  $Pm\bar{3}m$ , the face-centered cubic phase, is energetically preferred from 30 GPa

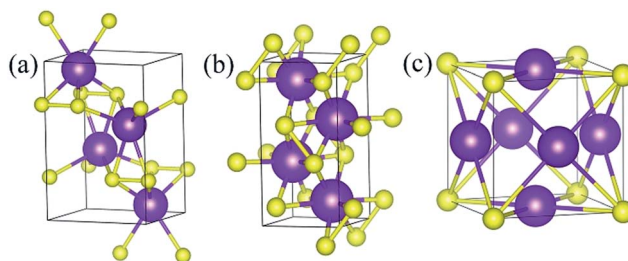


Fig. 3 Stable structures of  $\text{K}_x\text{S}$ : (a)  $Pm\bar{m}n$  KS at ambient pressure, (b)  $Pbam$  KS at 100 GPa, and (c)  $Pm\bar{3}m$   $\text{K}_3\text{S}$  at 50 GPa. The purple and yellow atoms are K and S, respectively.



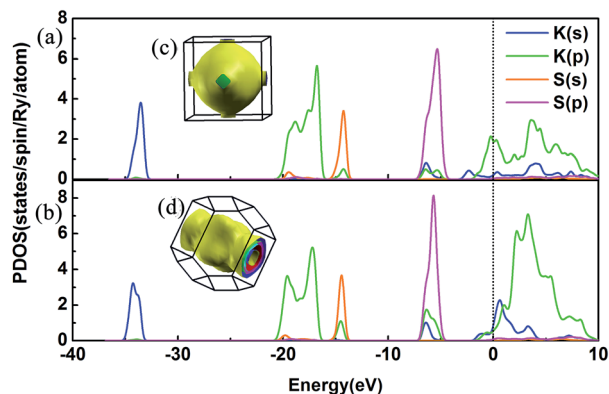


Fig. 4 PDOS and the three-dimensional Fermi surfaces of  $K_3S$ . (a) PDOS of  $Pm\bar{3}m$  at 50 GPa, (b) PDOS of  $I4/mmm$  at 100 GPa, (c) the three-dimensional Fermi surfaces of  $Pm\bar{3}m$  at 50 GPa, and (d) the three-dimensional Fermi surfaces of  $I4/mmm$  at 100 GPa. The black vertical dashed line indicates the Fermi energy.

to 55.7 GPa. The layer stacking sequence in every axis can be denoted by the repeated AB stacking. K atoms occupy the crystallographic 3c position with  $4/m\bar{m}.m$  symmetry sitting at the center of each cube face. S atoms occupy the crystallographic 1a position with  $m\bar{3}m$  symmetry around the cube corners as shown in Fig. 3(c). Each K atom is surrounded by the four nearest S atoms and the distance is 2.779 Å. The calculated structural parameters and Wyckoff positions for each phase are summarized in Table S1.† The mechanical property is one of the basic criteria when considering the structure stability. According to the mechanical stability criteria, the crystal deformation energy is positive which means the determinants of the elastic constants matrix  $C_{ij}$  should be positive.<sup>27</sup> It is noteworthy that negative values are not prohibited for  $C_{ij}$ .<sup>28</sup> To evaluate the mechanical stability of  $Pm\bar{3}m$ ,  $Pbam$ ,  $Pm\bar{3}m$ ,  $I4/mmm$ ,  $Cmcm$  and  $R\bar{3}m$ , the elastic constants were calculated and are listed in Table S2.† They all satisfy the Born–Huang criterion,<sup>29</sup> representing the stability of the mechanical property.

KS and  $K_2S$  are thermodynamically stable compounds throughout the entire pressure range we explored. At ambient

pressure,  $K_2S$  is the familiar stoichiometry in the  $K_xS$  system. We have predicted its phase sequence successfully by the ELocR<sup>21</sup> code, and account for the experimental results effectively.<sup>20</sup> Pressure can efficiently modify the compositional landscape, leading to materials with unprecedented stoichiometries that would not be expected from conventional wisdom based on chemical rules at ambient pressure. For instance, at ambient conditions, sodium chloride (NaCl) is the archetypical ionic compound in chemistry textbooks. Under pressure, different Na–Cl compounds such as  $Na_3Cl$ ,  $Na_2Cl$ ,  $Na_3Cl_2$ ,  $NaCl_3$ , and  $NaCl_7$ , which are clearly against our conventional wisdom, become thermodynamically stable.<sup>1,2</sup> Some other examples are seen in Li–B,<sup>30,31</sup> Ca–H,<sup>32</sup> and Si–C<sup>33</sup> systems at high pressure conditions. Interestingly, the unusual stoichiometry (1 : 1) KS compound is even stable thermodynamically and mechanically at ambient conditions. In order to judge its dynamical stability, the phonon band structure and partial phonon density of states (PHDOS) were calculated as shown in Fig. S2.† The absence of imaginary frequency modes in the entire Brillouin zone indicates the dynamic stability of  $Pm\bar{3}m$  (KS). Hence, KS, the totally counterintuitive chemical formula, may exist in nature theoretically.

We have discussed the mechanical and thermodynamical stability of the proposed phases and confirmed that they are all stable at the relevant pressure range. To understand the electronic properties of the various  $K_xS$  compounds, the electronic band structures, partial density of states (PDOS) and three-dimensional Fermi surfaces were calculated as depicted in Fig. 4 and S3.† From the band structures we found that all the stable phases at the different pressures are metallic due to several bands crossing the Fermi level, except for  $Pm\bar{3}m$  and  $Pbam$ . At ambient pressure, the band gap in  $Pm\bar{3}m$  is 1.432 eV, which reveals its nonmetallic character. Elevating the pressure above 3 GPa, the  $Pbam$  structure appears with nonmetallic features until 100 GPa. For  $K_3S$ , from the partial density of states (PDOS) in Fig. 4(a) and (b), the metallic character of  $Pm\bar{3}m$  and  $I4/mmm$  is confirmed by the high level of total electronic density distribution at the Fermi level. The majority of the occupied states come from the K(p) state, whereas the contribution from

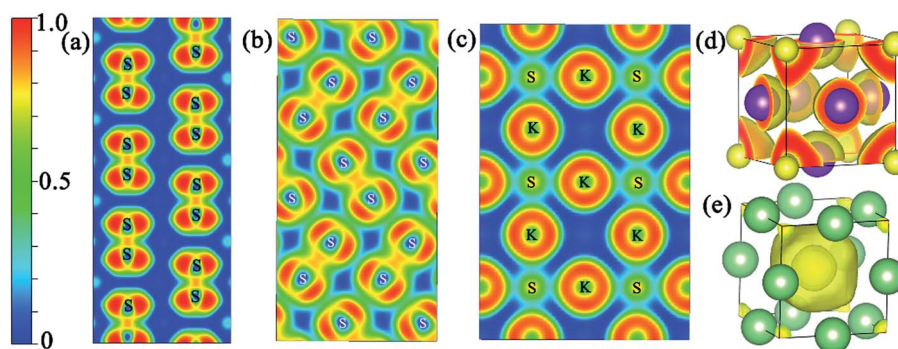


Fig. 5 The electron localization function of KS,  $K_2S$  and  $Li_3S$ . (a)  $Pm\bar{3}m$  2D ELF slice along the (011) plane at ambient pressure; (b)  $Pbam$  2D ELF slice along the (001) plane at 100 GPa; (c)  $Pm\bar{3}m$   $K_3S$  2D ELF slice along the (001) plane at 50 GPa; (d)  $Pm\bar{3}m$   $K_3S$  3D ELF map with the ELF values of 0.65 at 50 GPa; (e)  $Pm\bar{3}m$   $Li_3S$  3D ELF map with the ELF values of 0.65 at 500 GPa.  $Pm\bar{3}m$   $Li_3S$  3D ELF map with the ELF values of 0.65 at 500 GPa.



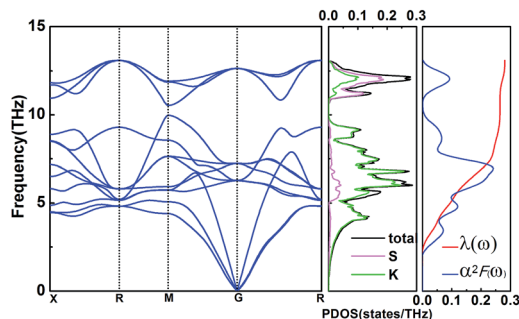


Fig. 6 Phonon dispersion curves, partial phonon density of states (PDOS), Eliashberg spectral function  $\alpha^2 F(\omega)$ , and the EPC  $\lambda$  for  $Pm\bar{3}m$  ( $K_3S$ ) at 50 GPa.

K(s), S(s) and S(p) to the states around the Fermi level is quite small in  $K_3S$ . This complex electronic band structure near the Fermi energy brings the rich and multiple Fermi surface feature, as displayed in Fig. 4(c) and (d).

In addition, the electron localization function (ELF) was calculated to analyze the nature of the chemical bonding and the unusual distribution of the valence electron localization function in the proposed structures at the relevant pressure range. It is a ratio from 0 to 1, and the values equal 1.0 and 0.5, reflecting the extremely strong localization and homogeneous electron distribution, respectively.<sup>34,35</sup> Fig. S4† shows the iso-surface value of 0.65 for the proposed structures. The valence electron localization around interstitial regions is found in  $Pm\bar{3}m$  ( $K_3S$ ),  $Pbam$  ( $K_3S$ ),  $I4/mmm$  ( $K_3S$ ),  $Cmcm$  ( $K_4S$ ), and  $R\bar{3}m$  ( $K_4S$ ), and is not found in  $Pm\bar{3}m$  ( $K_3S$ ). Fig. 5(a) and (b) show the two dimensional electron location function (2D ELF) of  $Pm\bar{3}m$  ( $K_3S$ ) and  $Pbam$  ( $K_3S$ ). The values around the positions of the  $S_2$  units are close to 0.75, revealing the covalent bond character. From the 2D ELF of  $Pm\bar{3}m$  ( $K_3S$ ) displayed in Fig. 5(c), we can see that the conductivity comes from connected regions where the value of ELF is about 0.5 between the K and S atoms. The ELF of  $Pm\bar{3}m$  ( $Li_3S$ ) at 500 GPa is calculated to compare with  $K_3S$  as shown in Fig. 5(e). Obviously, charges accumulate in the open interstitial regions in  $Li_3S$ . However, this phenomenon is not observed in  $Pm\bar{3}m$   $K_3S$  as displayed in Fig. 5(d).

To explore the potential superconductivity of  $Pm\bar{3}m$   $K_3S$ , the electron-phonon coupling (EPC) strength  $\lambda$  and logarithmic average phonon frequency  $\omega_{\log}$  have been investigated at 50 GPa by QUANTUM-ESPRESSO.<sup>26</sup> The Eliashberg phonon spectral function  $\alpha^2 F(\omega)$  can be obtained as below. It is described as:

$$\alpha^2 F(\omega) = \frac{1}{2\pi N(\epsilon_F)} \sum_{qv} \frac{\gamma_{qv}}{\omega_{qv}} \delta(\omega - \omega_{qv}) \quad (1)$$

hereinto the line width:

$$\gamma_{qv} = \lambda_{qv} \pi N(\epsilon_F) \omega_{qv}^2 \quad (2)$$

so, we can obtain  $\alpha^2 F(\omega)$ :

$$\alpha^2 F(\omega) = \frac{1}{2} \sum_{qv} \lambda_{qv} \omega_{qv} \delta(\omega - \omega_{qv}) \quad (3)$$

In this work,  $\alpha^2 F(\omega)$  is obtained by the integration of  $\omega_{qv}$  in the whole Brillouin zone. The heavier K atom from the low-frequency vibrational modes below about 8 THz contributes more to the total  $\lambda$  as shown in Fig. 6. Phonon-mediated superconductors are accurately described by the Migdal-Eliashberg theory,<sup>36,37</sup> and  $T_c$  can be estimated by the Allen-Dynes formula:<sup>38</sup>

$$T_c = \frac{\omega_{\log}}{1.2} \exp \left[ \frac{-1.04(1 + \lambda)}{\lambda - \mu^*(1 + 0.62\lambda)} \right] \quad (4)$$

which has been found to be highly accurate for many materials with  $\lambda < 1.5$ . We chose the better recommended values of the Coulomb pseudopotential  $\mu^*$  (0.1–0.13),<sup>39</sup> and the superconducting transition temperature  $T_c$  was estimated to nearly 0 K at 50 GPa. A recent theoretical study reported that  $Li_3S$  exhibits low- $T_c$  (0 K) in the  $Pm\bar{3}m$  phase and high- $T_c$  (80 K) in the  $Fm\bar{3}m$  phase, and it attributed the difference to interstitial charge localization, *i.e.*, charge localizing in the interstitial region is a limiting factor to conventional superconductivity.<sup>9</sup>  $K_3S$  has the same stoichiometry, space group and  $T_c$  as  $Li_3S$ , however, the mechanism of superconductivity is totally different. We attribute the low  $T_c$  to weak electron-phonon coupling. As expected, in  $K_3S$  and  $Li_3S$ ,  $T_c$  is dominated by  $\lambda$ . Then the variation of  $\lambda$  is analysed using the rigid-muffin-tin (RMT) theory of Gaspari and Gyorffy.<sup>40</sup> McMillan's strong coupling theory defines an electron-phonon coupling constant by

$$\lambda = \frac{N(\epsilon_F) \langle I^2 \rangle}{M \langle \omega^2 \rangle} = \eta N(\epsilon_F) \quad (5)$$

where  $\eta = \frac{\langle I^2 \rangle}{M \langle \omega^2 \rangle}$ .  $N(\epsilon_F)$  is the density of states (DOS) at the Fermi level,  $M$  is the atomic mass,  $\langle \omega^2 \rangle$  is a weighted average of

**Table 1** The calculated electronic density of states at the Fermi level  $N(\epsilon_F)$  (states/spin/Ry/atom), the logarithmic average phonon frequency  $\omega_{\log}$  (K), the average phonon frequency  $\langle \omega^2 \rangle^{1/2}$  (THz), the average over the Fermi surface of the electron-phonon matrix element  $\langle I^2 \rangle$  (eV Å<sup>-1</sup>),<sup>2</sup> the electron-phonon coupling parameters  $\lambda$ , and the superconducting critical temperatures  $T_c$  (K) of  $K_3S$  and  $Li_3S$  at 50 GPa and 500 GPa, respectively

	Phase	P (GPa)	$T_c$	$\omega_{\log}$	$\lambda$	$N(\epsilon_F)$	$\eta$	$\langle \omega^2 \rangle^{1/2}$	$\langle I^2 \rangle$
Present work	$Pm\bar{3}m$ ( $K_3S$ )	50	0.069	285.569	0.280	2.107	0.133	40.698	2.884
Present work	$Pm\bar{3}m$ ( $Li_3S$ )	500	0.044	814.923	0.250	0.668	0.375	141.074	25.120
Other calculations	$Pm\bar{3}m$ ( $Li_3S$ ) <sup>9</sup>	500	0	702	0.25	0.67	0.37		





the square of the phonon frequency, and  $\langle I^2 \rangle$  is an average over the Fermi surface of the electron–phonon matrix element. From Table 1,  $\eta$  plays an important role in  $\lambda$  which further influenced the low  $T_c$  in  $\text{Li}_3\text{S}$  and  $\text{K}_3\text{S}$ . With regard to  $\eta$ , it is believed that  $\eta$  is a factor about the lattice and its value is influenced by interstitial charge localization in  $\text{Li}_3\text{S}$ ,<sup>9</sup> *i.e.* charge localizing in the interstitial region led to a smaller  $\eta$ . The value of  $\eta$  in  $\text{K}_3\text{S}$  is smaller than that in  $\text{Li}_3\text{S}$ , nevertheless, there is no charge localizing in the interstitial region as shown in Fig. 5(c). We attribute the small  $\eta$  to the electron–ion matrix element  $\langle I^2 \rangle$ . In conclusion, the low  $T_c$  in  $\text{K}_3\text{S}$  is mainly influenced by electron–phonon coupling which is fully in contrast to the mechanism of interstitial charge localization which dominates the low  $T_c$  in the reported  $\text{Li}_3\text{S}$ .<sup>9</sup>

## Conclusions

In conclusion, a high-pressure phase diagram of K-rich  $\text{K}_x\text{S}$  systems was built from structure prediction simulations and first-principles calculations.  $\text{KS}$ , the totally counterintuitive chemical formula with extraordinary bonding and electronic properties, is predicted to be stable at atmospheric pressure. All of the S atoms of  $\text{KS}$  are in the form of  $\text{S}_2$  units with covalent bond character from the analyses of the electronic localization function. Further electron–phonon coupling calculations revealed that the  $T_c$  of  $\text{Pm}\bar{3}m$  ( $\text{K}_3\text{S}$ ) is approximately near to 0 K at 50 GPa. The mechanism of superconductivity in  $\text{Pm}\bar{3}m$   $\text{K}_3\text{S}$  was deeply investigated and compared with the reported  $\text{Pm}\bar{3}m$   $\text{Li}_3\text{S}$ . We attribute the low  $T_c$  to weak electron–phonon coupling in the  $\text{K}_3\text{S}$  compound.

## Conflicts of interest

There are no conflicts to declare.

## Acknowledgements

This work was supported by the National Natural Science Foundation of China (No. 51632002, 51572108, 11634004, 11174102, 11774119), the Program for Changjiang Scholars and Innovative Research Team in University (No. IRT\_15R23), the 111 Project (No. B12011), the National Fund for Fostering Talents of Basic Science (No. J1103202), and the Development Program of Science and Technology of Jilin Province, China (No. 20150312002ZG). Parts of the calculations were performed in the High Performance Computing Center (HPCC) of Jilin University.

## References

- W. Zhang, A. R. Oganov, A. F. Goncharov, *et al.*, *Science*, 2013, **342**, 1502–1505.
- J. I. Insa, *Science*, 2013, **342**, 1459–1460.
- X. Dong, A. R. Oganov, A. F. Goncharov, *et al.*, *Nat. Chem.*, 2017, **9**, 440–445.
- X. Jin, X. J. Chen, T. Cui, H. K. Mao, H. Zhang, Q. Zhuang, K. Bao, D. Zhou, B. Liu, Q. Zhou and Z. He, *Proc. Natl. Acad. Sci. U. S. A.*, 2016, **113**, 2366–2369.
- J. B. Neaton and N. W. Ashcroft, *Nature*, 1999, **400**, 141–144.
- T. Matsuoka and K. Shimizu, *Nature*, 2009, **458**, 186–189.
- Y. Yao, S. T. John and D. D. Klug, *Phys. Rev. Lett.*, 2009, **102**, 115503.
- Y. Ma, M. Erements, A. R. Oganov, *et al.*, *Nature*, 2009, **458**, 182–185.
- C. Kokail, C. Heil and L. Boeri, *Phys. Rev. B*, 2016, **94**, 060502.
- P. G. Bruce, S. A. Freunberger, L. J. Hardwick and J. Tarascon, *Nat. Mater.*, 2012, **11**, 19–29.
- H. Momida, T. Yamashita and T. Oguchi, *J. Phys. Soc. Jpn.*, 2014, **83**, 124713.
- H. Khachai, R. Khenata and A. Bouhemadou, *Solid State Commun.*, 2008, **147**, 178–182.
- R. D. Eithiraj, G. Jaiganesh and G. Kalpana, *Phys. Status Solidi A*, 2007, **244**, 1337–1346.
- J. C. Schön, Ž. Čančarević and M. Jansen, *J. Chem. Phys.*, 2004, **121**, 2289.
- H. Khachai, R. Khenata and A. Bouhemadou, *J. Phys.*, 2009, **21**, 095404.
- E. Zintl, A. Harder and B. Dauth, *Z. Elektrochem. Angew. Phys. Chem.*, 1934, **40**, 588–593.
- A. Grzechnik, A. Vagas, K. Syassen, L. Loa, M. Hanfland and M. Jansen, *J. Solid State Chem.*, 2000, **154**, 603–611.
- A. Vegas, A. Grzechnik, K. Syassen, L. Loa, M. Hanfland and M. Jansen, *Acta Crystallogr., Sect. B: Struct. Sci.*, 2001, **57**, 151–156.
- D. Santamaria-Perez, A. Vegas, C. Muehle and M. Jansen, *Acta Crystallogr., Sect. B: Struct. Sci.*, 2011, **67**, 109–115.
- Y. Li, X. Jin, T. Cui, Q. Zhuang, Q. Lv, G. Wu, X. Meng, K. Bao, B. Liu and Q. Zhou, *RSC Adv.*, 2017, **7**, 7424–7430.
- The code for crystal structural prediction and analysis is based on the evolutionary local random computational method, and is developed by our group. Some details have been provided in the ESI.†
- G. Kresse and J. Furthmüller, *Phys. Rev. B: Condens. Matter Mater. Phys.*, 1996, **54**, 11169–11186.
- J. P. Perdew, K. Burke and M. Ernzerhof, *Phys. Rev. Lett.*, 1997, **77**, 3865–3868.
- P. E. Blöchl, *Phys. Rev. B: Condens. Matter Mater. Phys.*, 1994, **50**, 17953–17979.
- S. J. Clark, M. D. Segall and C. J. Pickard, *Z. Kristallogr. - Cryst. Mater.*, 2005, **220**, 567–570.
- P. Giannozzi, S. Baroni, N. Bonini, M. Calandra, R. Car, C. Cavazzoni, D. Ceresoli, G. L. Chiarotti, M. Cococcioni, I. Dabo, A. Dal Corso, S. de Gironcoli, S. Fabris, G. Fratesi, R. Gebauer, U. Gerstmann, C. Gougoussis, A. Kokalj, M. Lazzeri, L. Martin-Samos, N. Marzari, F. Mauri, R. Mazzarello, S. Paolini, A. Pasquarello, L. Paulatto, C. Sbraccia, S. Scandolo, G. Sclauzero, A. P. Seitsonen, A. Smogunov, P. Umari and R. M. Wentzcovitch, *J. Phys.: Condens. Matter*, 2009, **21**, 395502.
- J. F. Nye, *Physical properties of crystals: their representation by tensors and matrices*, Oxford Univ. Press, Oxford, 1985, pp. 142–143.



- 28 J. P. Perdew and K. Burke, *Phys. Rev. Lett.*, 1997, **77**, 3865–3868.
- 29 Z. Wu, E. Zhao and H. Xiang, *Phys. Rev. B: Condens. Matter Mater. Phys.*, 2007, **76**, 054115.
- 30 F. Peng, M. Miao, H. Wang, Q. Li and Y. Ma, *J. Am. Chem. Soc.*, 2012, **134**, 18599–18605.
- 31 A. Hermann, A. McSorley, N. W. Ashcroft and R. Hoffmann, *J. Am. Chem. Soc.*, 2012, **134**, 18606–18618.
- 32 H. Wang, S. T. John, K. Tanaka, T. Iitaka and Y. Ma, *Proc. Natl. Acad. Sci. U. S. A.*, 2012, **109**, 6463–6466.
- 33 G. Gao, N. Ashcroft and R. Hoffmann, *J. Am. Chem. Soc.*, 2013, **135**, 11651–11656.
- 34 A. D. Becke and K. E. Edgecombe, *J. Chem. Phys.*, 1990, **92**, 5397–5403.
- 35 J. K. Burdett and T. A. McCormick, *J. Phys. Chem. A*, 1998, **102**, 6366–6372.
- 36 A. B. Migdal, *J. Exp. Theor. Phys.*, 1958, **34**, 996.
- 37 G. M. Eliashberg, *J. Exp. Theor. Phys.*, 1960, **11**, 696.
- 38 P. B. Allen and R. C. Dynes, *Phys. Rev. B: Solid State*, 1975, **12**, 905–922.
- 39 N. W. Ashcroft, *Phys. Rev. Lett.*, 2004, **92**, 187002.
- 40 G. D. Gaspari and B. L. Gyorffy, *Phys. Rev. Lett.*, 1972, **28**, 801–805.

